

The chromospherically active binary star EI Eridani

I. Absolute dimensions

A. Washuettl^{1,2*}, K. G. Strassmeier^{1*}, T. Granzer¹, M. Weber^{1*}, and K. Oláh²

¹ Astrophysical Institute Potsdam (AIP), An der Sternwarte 16, D-14482 Potsdam, Germany
e-mail: awashuettl/kstrassmeier/tgranzer/mweber@aip.de

² Konkoly Observatory, P.O. Box 67, H-1525 Budapest, Hungary
olah@konkoly.hu

The dates of receipt and acceptance should be inserted later

Key words stars: activity – stars: individual: EI Eri – stars: late-type – binaries: close

We present a detailed determination of the astrophysical parameters of the chromospherically active binary star EI Eridani. Our new radial velocities allow to improve the set of orbital elements and reveal long-term variations of the barycentric velocity. A possible third-body orbit with a period of ≈ 19 years is presented. Absolute parameters are determined in combination with the *Hipparcos* parallax. EI Eri's inclination angle of the rotational axis is confined to $56^\circ 0 \pm 4^\circ 5$, its luminosity class IV is confirmed by its radius of $2.37 \pm 0.12 R_\odot$. A comparison to theoretical stellar evolutionary tracks suggests a mass of $1.09 \pm 0.05 M_\odot$ and an age of ≈ 6.15 Gyr. The present investigation is the basis of our long-term Doppler imaging study of its stellar surface.

© 2006 WILEY-VCH Verlag GmbH & Co. KGaA, Weinheim

1 Introduction

EI Eridani = HD 26337 (G5 IV, $P_{\text{rot}} = 1.947$ days, $V = 7.1$ mag) is a rapidly rotating ($v \sin i = 51 \text{ km s}^{-1}$) active, non-eclipsing, single-lined spectroscopic binary star and as such a typical RS CVn star. RS CVn stars are close but detached binary systems that rotate synchronously due to tidal forces. This anomalously fast rotation is believed to be responsible for the high activity level found on these stars and constitute valuable laboratories to study the evolved Sun in action.

Ca II H and K emission – the classical fingerprint of magnetic activity – on EI Eri was first noted by Bidelman & MacConnell (1973) and confirmed later by Fekel (1980) who classified it as moderate in strength, class C on the qualitative emission scale by Hearnshaw (1979). Line-profile data of Ca II H and K and H α emission lines were obtained by Strassmeier et al. (1990) and Fernandez-Figueroa et al. (1994). Fekel et al. (1982) classified EI Eri as a single-lined RS CVn star when they detected its light variability, with an amplitude being almost $0^{\text{m}}2$ in V and a photometric and orbital period of around two days. Later, Fekel et al. (1986) determined the orbital period to be $1^{\text{d}}9472$ while Hall et al. (1987) detected a photometric period of 1.945 ± 0.005 days from UBV photometry. The H α line is in absorption, as in most RS CVn stars, but highly filled in with chromospheric

emission (see Smith & Bopp 1982) and quite variable in strength (Fekel et al. 1986; Zboril et al. 2005). These variations are assumed to be caused by rotational modulation of the chromospheric H α emission, presumably due to evolving plage regions on the stellar surface moving in and out of sight. Fekel et al. (1987), Pallavicini et al. (1992) and Randich et al. (1993) reported the presence of moderate amounts of lithium. Hall et al. (1987) already noted season-to-season changes in the photometric period ($\sim 1\%$), in the light-curve amplitude ($0^{\text{m}}07 - 0^{\text{m}}20$) and in the mean brightness ($\sim 10\%$), likely indicating latitude and/or longitude changes of the location of starspots. Strassmeier et al. (1989) report seasonal changes of the photometric period of 0.043 days within three seasons. Rodono & Cutispoto (1992) suggested a possible cycle period of about 10 years. Strassmeier et al. (1997) summarized the first 16 years of photometric data and found a possible 11 ± 1 years cycle of the mean brightness while (Oláh & Strassmeier 2002) refined this to be 12.2 years. Recent observations in other spectral regions were presented by Osten et al. (2002), García-Sánchez et al. (2003) and Cardini (2005).

With its large rotational velocity and an intermediate inclination, EI Eri is an ideal candidate for *Doppler imaging*. This technique (see Rice 2002) allows the reconstruction of the surface spot distribution of rapidly rotating stars by using the relation between wavelength position across an absorption line and spatial position across the stellar disk. However, the rotational period of 1.947 days makes it difficult to obtain spectral coverage for a complete rotation period, and ideally, when using a single observing site, three

* Visiting Astronomer, Kitt Peak National Observatory and National Solar Observatories, National Optical Astronomy Observatory, which is operated by the Association of Universities for Research in Astronomy, Inc. (AURA) under cooperative agreement with the National Science Foundation.

weeks of observations are needed to provide good phase coverage for a Doppler image of EI Eridani.

Doppler images for the 1984–87 period were presented by Hatzes & Vogt (1992). Strassmeier (1990) and Strassmeier et al. (1991) published Doppler images from 1987–88. All images show a large asymmetric spot at the pole or at high latitudes with several appendages and occasionally equatorial spots. The polar spot is long lived but exhibits significant changes of its size and shape, while the equatorial spots change within weeks. Furthermore, Donati et al. (1997) detected a clear Zeeman signature of the magnetic field of the primary star.

In this paper, we present spectroscopic and photometric observations obtained at KPNO and NSO in the years 1988–1998 and with the MUSICOS 98 campaign, and perform an investigation of the absolute dimensions of EI Eri in order to prepare for a Doppler imaging study. In two forthcoming papers, we will present our Doppler imaging results and address the question of spot lifetimes, long-term cyclic behavior (Washuettl et al. 2009b, hereafter “paper II”) and differential rotation (Washuettl et al. 2009a, hereafter “paper III”).

2 Observations and data reduction

All our spectroscopic data were obtained from four observing runs with the Coudé Feed telescope at Kitt Peak (March 1994, February 1995, January 1996, December 1997), one dedicated visitor observing run at the McMath–Pierce Telescope (NSO) in Nov/Dec. 1996, from the McMath/NSO synoptic program (1988–1995) and from the MUSICOS campaign 1998. The observing logs and radial velocities from KPNO and NSO are given in Table A which is available only in electronic form. The MUSICOS 98 spectroscopic data will be presented in a forthcoming dedicated paper. A summary of all observing runs is shown in Table 1.

2.1 Kitt Peak National Observatory (KPNO)

The KPNO data were obtained with the 0.9m Coudé feed telescope. For the 1994 run (March 4 – 18; hereafter: “CF94”) and the 1995 run (Feb. 22 – March 7; “CF95”) we used the 800×800 TI-5 CCD chip ($15 \mu\text{m}$ pixels), grating A, camera 5, the long collimator and a $280 \mu\text{m}$ slit giving a resolving power ($\lambda/\Delta\lambda$) of 36 000 at a wavelength of 6420 \AA (the FWHM of an unblended Th–Ar comparison lamp line was about 1.7 pixel; dispersion was $0.1 \text{ \AA}/\text{px}$). The useful wavelength range of the resulting spectra is 80 \AA . For the 1996 run (Jan. 11 – 25; “CF96”) we used the 1000×3000 pixel Ford CCD (F3KB chip, $15 \mu\text{m}$ pixels; two pixels each were binned), with an otherwise identical spectrograph setup. F3KB enables a much larger wavelength region ($\sim 320 \text{ \AA}$ from $\lambda 6335$ to $\lambda 6655$) at a spectral dispersion of $\approx 0.104 \text{ \AA}$ per pixel. The resolving power is 24 000 at 6420 \AA as measured by the FWHM of a Th–Ar line of about 2.6 pixel. An additional observing run primarily dedicated to

Table 2 Radial velocity standard stars. The velocity values are from Scarfe et al. (1990) except 59 Ari which is from Wilson (1953).

	α Tau	α Ari	β Gem	16 Vir	59 Ari	β Lep
HD	29139	12929	62509	107328	20618	36079
v_r	54.25	-14.51	3.23	36.48	-0.1	-13.5
σ_{v_r}	0.08	0.11	0.15	0.04	?	0.1
NSOsyn					*	
NSO 96		*				
KP 94				*		
95	*			*		
96	*		*	*		
97		*	*	*		
MUSICOS	*					*

EI Eridani was undertaken in winter 1997/98 (Dec. 26 – Jan. 15; “CF97”). This time, we employed the TI-5 chip again, seeking the better resolution. The FWHM of a Th–Ar line was measured to be 2.0 pixel, corresponding to a resolving power of approximately 30 000.

A typical night of observations includes 20–40 biases, 10–20 flat-field images, and 2–3 integrations of a thorium–argon hollow cathode lamp for establishing the wavelength scale, at least one at the beginning and one at the end of each night, but usually every three hours. Additionally, at least one observation from a choice of four radial velocity standard stars (see Table 2) was taken per night. Neither the TI-5 CCD nor the F3KB CCD show discernible signs of fringing at the wavelength of our observations. Consequently, no attempts were made to correct for it other than the standard flat-field division.

Data reduction was done using the NOAO/IRAF software package and followed our standard procedure as described in Weber & Strassmeier (1998) which includes bias subtraction, flat fielding, and optimal aperture extraction. All spectra were checked for narrow telluric water lines. These lines can be blended with Doppler imaging lines and produce misleading artifacts in the surface maps. The spectra of a rapidly rotating ($v \sin i \approx 300 \text{ km s}^{-1}$) hot B-star revealed these telluric lines and were compared with the spectra of EI Eri. Sporadic telluric water-vapor lines were found in this wavelength region, but fortunately, in most cases no blend of a water line with a Doppler imaging line occurred, and no corrections had to be applied to the line profiles used for further analysis. Special care was exercised during the continuum fitting process. A low-order polynomial was sufficient to find a satisfactory continuum solution. Exposure length was typically 45 minutes but up to 60 minutes in case of thin cirrus.

With this integration time we achieved a signal-to-noise ratio of up to 400:1.

Table 1 Overview of all observing runs.

Site	Acronym	Date	HJD (24+)	n^a	Detector	Disp. [Å/px]	ThAr FWHM [px]	$\lambda/\Delta\lambda$ [Å]
NSO	NSOsyn	1988, Nov 16 – 1995, Dec 28	47481.9 – 50079.9	225	TI-4	0.096	1.6	42 000
	M96	1996, Nov 01 – 1996, Jan 08	50388.9 – 50457.8	58	TI-4	0.118	1.9	29 000
KPNO	CF94	1994, Mar 05 – 1994, Mar 15	49416.6 – 49426.6	3	TI-5	0.106	1.7	36 000
	CF95	1995, Feb 21 – 1995, Mar 06	49770.6 – 49783.6	5	TI-5	0.106	1.7	36 000
	CF96	1996, Jan 10 – 1996, Jan 24	50093.6 – 50107.8	24	F3KB	0.104	2.6	24 000
	CF97	1997, Dec 27 – 1997, Jan 15	50809.6 – 50828.9	57	TI-5	0.1055	2.0	30 000
MUSICOS ^b		1998, Nov 21 – 1998, Dec 13	51139.4 – 51159.6	95	(various)			

^a ... Number of spectra

^b ... The results from the MUSICOS campaign will be presented in a dedicated paper.

Table 3 Original and improved orbital elements for EI Eri. The original values are from Strassmeier (1990) except T_0 which is from Fekel et al. (1987) and M_1 from Nordström et al. (2004). The numbers in brackets denote the error in the last digit(s).

Orbital element	Original	Improved
P [days]	1.947227 (8)	1.9472324 (38)
T_0 [HJD]	2 446 074.384	2 448 054.7109 (5)
γ [km s ⁻¹]	17.6 (2)	21.64 (16)
K_1 [km s ⁻¹]	27.4 (3)	26.83 (23)
e (assumed)	0.0	0.0
$a_1 \sin i$ [km]	733000 (9000)	718400 (6200)
$f(M)$ [M _⊙]	0.00415 (15)	0.00391 (10)
M_1 [M _⊙] ^a	1.10 (12)	1.09 (5)
M_2 [M _⊙] ^b	–	0.23 (4)
K_2 [km s ⁻¹] ^c	–	128 (25)
$a_2 \sin i$ [km] ^c	–	3.4 (7) · 10 ⁶
a [km] ^d	–	5.0 (9) · 10 ⁶
Standard error of an observation of unit weight [km s ⁻¹]		3.2

^a ... estimated using evolutionary tracks; see §4.5.

^b ... calculated using $f(M)$, assuming $i = 56.0 \pm 4.5^\circ$.

^c ... using the estimations of M_1 and M_2 .

^d ... assuming $i = 56.0 \pm 4.5^\circ$.

2.2 National Solar Observatory (NSO)

Our NSO data were obtained with the 1.5 m McMath-Pierce solar telescope during a regular visitor observing run covering 70 nights (from November 1, 1996, to January 8, 1997; hereafter: “M96”), as well as from the synoptic nighttime program (Smith & Giampapa 1987) from 1988 till 1995. The 58 spectra from the M96 observing run were taken using the 4.6m vertical Czerny-Turner stellar spectrograph (Smith & Jaksha 1984) with the Milton-Roy grating #1 and the 105-mm transfer lens together with the 800×800 TI-4 CCD camera (15 μm pixels) at a dispersion of 0.118 Å/pixel.

Table 4 Suggestions for a possible third body orbit. The index “1-2” refers to the inner binary system.

Orbital element	circular	eccentric
P [days]	6700 ± 500	6700 ± 500
T_0 [HJD] (adopted)	2 442 500	2 443 300
γ [km s ⁻¹]	21.0	19.4
K_{1-2} [km s ⁻¹]	4 ± 1	5.8 ± 1
e (assumed)	0.0	0.4
ω [°]	–	60
$a_{1-2} \sin i$ [km]	3.7 ± 1.0 · 10 ⁸	5.3 ± 2.3 · 10 ⁸
$f(M)$ [M _⊙]	0.044 ± 0.035	0.13 ± 0.18
M_{1-2} [M _⊙]	1.32 ± 0.07	1.32 ± 0.07
M_3 [M _⊙] ^a	0.7 ± 0.6	1.1 ± 1.7
K_3 [km s ⁻¹] ^b	8 ± 7	7 ± 11
$a_3 \sin i$ [km] ^b	7 ± 7 · 10 ⁸	6 ± 10 · 10 ⁸
a [AU] ^c	9 ± 6	9 ± 8
Standard error of an observation of unit weight [km s ⁻¹]	3.3	1.6

^a ... calculated using $f(M)$, assuming $i = 56.0 \pm 4.5^\circ$.

^b ... using the estimations of M_{1-2} and M_3 .

^c ... assuming $i = 56.0 \pm 4.5^\circ$.

The mean FWHM of Thorium-Argon emission lines was around 1.9 pixels, corresponding to a resolving power of ~29 000. The spectra were generally recorded in a sequence of 3×15 minutes exposures and added up later including cosmic ray removal. The integration time of the combined spectra was between 20 and 60 min. The observations covered a wavelength range of about 45 Å from 6410 to 6460 Å and included three lines suitable for Doppler imaging: Fe I 6411, Fe I 6430 and Ca I 6439. The average signal-to-noise ratio is ≈150:1. Data reduction was done again using the NOAO/IRAF software package in the same way as for the KPNO coude feed data. Usually, 20 flat-field exposures with a Tungsten lamp were taken at the beginning and at the end of each night, about three exposures of a Thorium-

Argon reference lamp and at least one observation of the IAU radial velocity standard star α Ari were taken each night. The 58 spectra in M96 cover together 35.4 consecutive stellar rotations.

The other part of the NSO observations were part of the synoptic night-time program at the McMath-Pierce telescope during the years 1988 till 1995. Over the course of these seven years, a total of 225 spectra was acquired. The same 800×800 TI-4 was applied in conjunction with the Milton-Roy (B&L) grating #1 but with a significantly better dispersion of 0.096 \AA/px and an average FWHM of a comparison lamp emission line of 1.6 px , thus increasing the resolution to $R=42\,000$, giving an effective wavelength resolution of 0.15 \AA (see Strassmeier et al. 1991). The signal-to-noise ratio of the NSO synoptic spectra reaches in most cases 300:1.

2.3 Photometric observations

Photometric data were provided by the Amadeus (T7) 0.75m Vienna-Observatory Automatic Photoelectric Telescope (APT), part of the University of Vienna twin APT, now at Washington Camp in southern Arizona (Strassmeier et al. 1997), previously, before summer 1996, on Mt. Hopkins. The observations were made differentially with respect to HD 25852 as the comparison star ($V = 7^m 83$; since Nov. 8, 1996) and HD 26409 as check star ($V = 5^m 448$). All photometry was transformed to match the Johnson-Cousins $V(RI)_C$ system (see Granzer et al. 2001, §4). In addition, older photometric observations back to 1980 were used from the literature (see Strassmeier et al. 1997, Table 5).

3 Orbit analysis

3.1 Radial velocities and spectroscopic orbit

Radial velocities (RVs) were determined from cross-correlations with spectra of a radial velocity standard star observed during the same night. Since EI Eri is a single-lined spectroscopic binary, only the RV of the primary component can be measured. No RV information is available for the secondary star. The cross correlations were computed using IRAF's `fxcor` routine (see Fitzpatrick 1993), which fits a Gaussian to the cross-correlation function to determine the central shift. Several different IAU standards were used, see Table 2. Their RVs were adopted from the work of Scarfe et al. (1990) except 59 Ari which is from Wilson (1953).

Orbital elements were derived with the differential-correction program of Barker et al. (1967), as modified and described by Fekel et al. (1999). We obtained altogether 354 new RVs for the primary component of EI Eri, 89 of which are from our four dedicated KPNO Coudé Feed observing runs, 58 from the one dedicated visitor observing run at NSO/McMath (M96). Additionally, 178 from the NSO

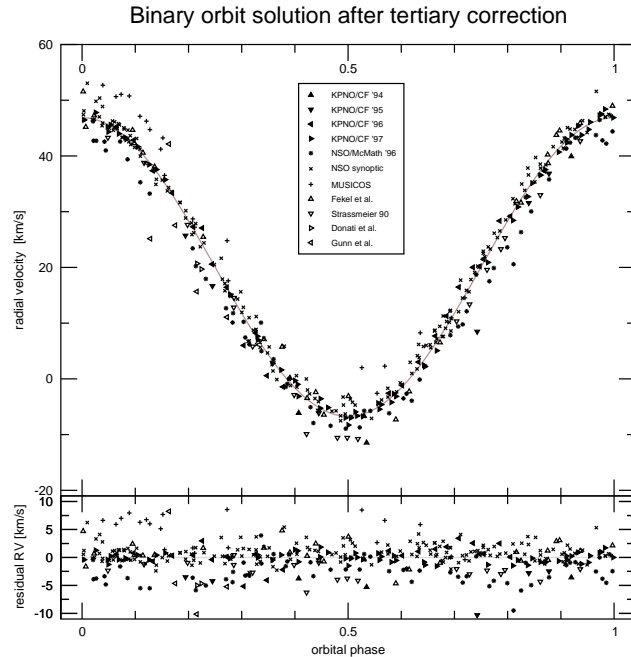


Fig. 1 Observed and computed radial velocity curve. The line is the orbital solution from the elements in Table 3. The lower panel gives the residual radial velocities, i.e. the difference between the observed radial velocities and the theoretical curve from the orbital solution. A third body in a wide orbit was taken into account.

synoptic night-time program (1988–1995) and 29 from the MUSICOS 98 campaign. Additionally, 55 older RVs were found in the literature: 27 from Fekel et al. (1987), 21 from Strassmeier (1990), five from Gunn et al. (1996), and two from Donati et al. (1997). Fekel & Strassmeier used the RV standards α Tau, β Gem, 10 Tau and ι Psc with the RV values from the older IAU list of RV standard stars (Pearce 1955). Therefore, they were corrected to match the values by Scarfe et al. (1990). The values by Gunn et al. (1996) and Donati et al. (1997) were not used for calculating the orbit.

Table 3 lists the improved orbital elements from minimized $O-C$ residuals using all available RVs. The orbit is plotted in Fig. 1. Our final orbital elements converged at an eccentricity so close to zero that, in accordance with the criteria established by Lucy & Sweeney (1971), a formal zero-eccentricity solution was adopted. The standard error of an observation of unit weight is 3.2 km s^{-1} . Phases of all line profiles were then computed using our revised ephemeris

$$\text{HJD} = 2,448,054.7109 + 1.9472324 \times E. \quad (1)$$

Our revised orbital elements agree very well with the older ones from Fekel et al. (1987), except for γ (see §3.2).¹

¹ Donati et al. (1997) pointed out that the RVs they measured at two epochs are in strong disagreement with the ephemeris from Strassmeier (1990). Gunn et al. (1996) also report that their five RVs diverge significantly; they suspect the high rotational velocity to be responsible for the large discrepancies. As a matter of fact, Strassmeier's T_0 value for his or-

3.2 EI Eri – a triple-star system?

By obtaining precise radial velocity measurements, more and more active close binary stars turn out to be members of triple systems, e.g. BY Dra (Zuckerman et al. 1997), XY UMa (Chochol et al. 1998), HU Vir (Fekel et al. 1999), UX Ari (Duemmler & Aarum 2001). Also for EI Eri, we noticed that the barycentric velocity γ seemed to have increased since the early observations in the 1980s by up to 8 km s^{-1} in the mid-1990ies. In order to examine whether the system is possibly a triple star, we calculate an orbit for several data subsets just varying the barycentric velocity γ and, for comparison, also the amplitude of the semi-major axis K_1 (Fig. 2). The γ values of EI Eri vary between 15.7 and 26.7 km s^{-1} ($> 3\sigma$) with an average error of 0.8 km s^{-1} . It is seen that γ shows an obvious trend over the period of 20 years, which is not the case for K_1 . A possible explanation could be the use of different RV standard stars and the use of different instrumental configurations and reduction techniques. The standards used for measuring the RV shifts for the KPNO, NSO and MUSICOS observing runs are listed in Table 2. Strassmeier (1990) and Fekel et al. (1987) largely used the same standard stars. For the observing runs by Fekel et al. (1987), Strassmeier (1990) and our CF97 run, two of the three RV standards used are in common. However, γ differs by 4 km s^{-1} which is about 10σ . The NSO data, all taken with the same instrumental setup and the same RV standard star (except M96) vary by 9 km s^{-1} (mean deviation: $2\text{--}3 \text{ km s}^{-1}$). A cross correlation of all RV standard stars used (NSO, KPNO and MUSICOS) uncovers a mean standard deviation of 0.82 km s^{-1} for the RV standard stars of the individual observing runs, while the mean RV values of the blocks exhibit a standard deviation of 1.69 km s^{-1} (2.1σ). Only the observing blocks CF96 (3.2σ), CF97 (5.6σ) and MUSICOS (3.6σ) deviate more than 2σ . During the same period, γ varies on average by 7σ . We conclude that the γ variations are not due to stochastic variations of the RV standard stars (as caused by, e.g., different instrumental setups).

As a test, we take the (observed-minus-computed) RV residuals of the orbit solution of the primary-secondary system presented in Fig. 1 and perform a period search on them. No clear and outstanding peak is found in the range $20 \text{ days} \leq P \leq 1000 \text{ days}$. However, several weak periods are visible. The strongest are 6667 (0.000150), 2950 (0.000339), 1626 (0.000615), 301 (0.00332), 216 (0.00463), 203 (0.00493), 130 (0.00769) and 96 days (0.0104 c/d). After pre-whitening, i.e. subtracting the $f_0=0.000150 \text{ c/d}$ signal from the residual RVs, the power spectrum does not show any distinct period any more. When subtracting any of the other periods, the 6667 d period remains intact. This means that the 6667 days period is the only signal present in the residual data. The next two peaks

bital solution seems to have been confused possibly due to a typing mistake as it does not give sensible results for his own RVs. Accordingly, both Donati's and Gunn's RV values are in perfect agreement with the previous ephemeris of Fekel et al. (1987).

Orbit: gamma variations 1979 - 1998

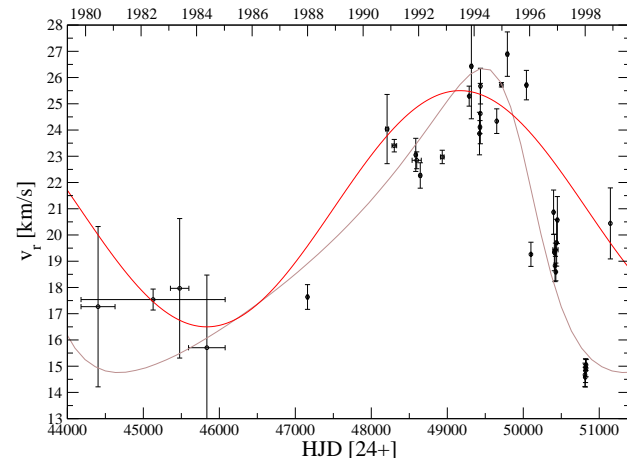


Fig. 2 Variations of the barycentric velocity γ . The bars in the axis of abscissae (x) denote the time span of the data used for calculating the orbit. The bars in the axis of ordinates (y) are the error bars of the respective γ values. The curve shows two suggestions for tertiary orbits according to the orbital parameter in Table 4.

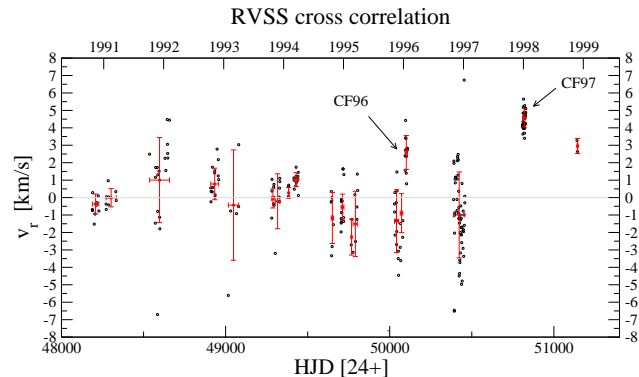


Fig. 3 Cross correlation of all used radial velocity standard star spectra. The dots are the radial-velocity offsets for all individual RV standard stars (RVSS). The dots with bars are the mean RV value for each observing block (corresponding to the suborbits in Fig. 2); the bars in the axis of abscissae (x) denote the time span of the respective observing block, the bars in the axis of ordinates (y) are the standard deviations of the RV values of the respective observing block.

can be explained as the second and third peak $2f_0$ and $4f_0$ of the 6667 d period, the other ones come from the structure of the window function. Of course, this period is very close to the total length of our data sample and therefore uncertain and possibly spurious.

Assuming a third component as the origin of these variations, we can calculate an orbit of this potential tertiary star which would be surrounding the inner binary system in a wide orbit with a period of around 20 years and an amplitude K_{1-2} of $\approx 4 \pm 1 \text{ km s}^{-1}$, leading to a $f(M)$ of $0.044 \pm 0.035 M_\odot$ and a $a_{1-2} \sin i$ of $3.7 \pm 1.0 \cdot 10^8 \text{ km}$ (Ta-

ble 4, left column; the right column presents an alternative eccentric orbit). All three values shrink in case of non-zero eccentricity. In §4.5, we will discuss the mass of a potential tertiary.

4 Astrophysical parameters of EI Eri

4.1 Effective temperature

Bidelman & MacConnell (1973) classified EI Eri as G5 IV from objective-prism plates. Harlan (1974) classified it as G2 IV-V, while Abt (1986) assumed a “weak-lined” G5 V classification from photometric indices. Cutispoto (1995) finds its UBVR colors consistent with a G5 IV + G0 V system. The classification of G5 IV is also favored by Fekel et al. (1986) on the basis of high-resolution spectra.

The effective temperature of EI Eri can be estimated by comparing the observed $U - B$, $B - V$, $V - R_C$ and $V - I_C$ colours (which are 0^m13 , 0^m67 , 0^m40 and 0^m77 , respectively; Cutispoto 1995) to synthetic and empirical values from colour-temperature transformation lists. For EI Eri’s $B - V$ value of 0^m67 , Flower (1996) lists a temperature of 5653 K. Comparing with ATLAS-9 model atmospheres (Kurucz 1993)², we find our $U - B$ and $B - V$ values to be consistent with a temperature of $T_{\text{eff}} = 5500$ K for metallicities between -0.5 and -1.0 dex which is required by the reconstruction of the line profiles (see paper II). Solar abundances would yield 250 K higher temperature. $V - I_C$ and $V - R_C$ yield temperatures in-between 5500 and 5750 K. Schmidt-Kaler (1982) lists 5770 K for $B - V = 0^m68$ for luminosity class V. Randich et al. (1993) derived a T_{eff} of 5700 K using a spectrum synthesis analysis. Nordström et al. (2004) list an effective temperature of 5408 K (from the calibration of Alonso et al. 1996). We finally adopt a value of 5500 K which is supported by our Doppler imaging results (Strassmeier et al. 1991; Washuettl et al. 2001, 2009b).

The above temperatures are formally for the combined EI Eri binary star. However, no spectral lines from the secondary are seen which means that the continuum ratio must be larger than about a factor 10. According to our orbit, M_2 amounts to $0.23 \pm 0.04 M_{\odot}$ (see §4.5) which corresponds to a spectral type of M4-5 V and to $L_2 \approx 1-2 \cdot 10^{-2} L_{\odot}$ (assuming a dwarf). Compared to the primary ($L_1 = 4.6 L_{\odot}$), the secondary contributes only 2–4% of the total light and can therefore be neglected for the Doppler imaging study.

4.2 Rotational broadening and stellar radius

The projected equatorial velocity, $v \sin i$, was estimated by Fekel et al. (1986) to be $50 \pm 3 \text{ km s}^{-1}$ while Hatzes & Vogt (1992) and Donati et al. (1997) gave $50 \pm 1 \text{ km s}^{-1}$ and $51 \pm 1 \text{ km s}^{-1}$, respectively. For the present investigation, we use the Doppler-imaging technique to verify and slightly improve the $v \sin i$ value. Doppler imaging is very sensitive

² <http://ccp7.dur.ac.uk/ccp7/Atlas/colours/ubvm05k2.dat>

Table 5 Original and improved astrophysical parameters of EI Eri. Orbital values are listed separately in Table 3.

Parameter	Original value	Improved value (this paper)
Spectral type	G5 IV ^a	G5 IV + (M4-5 V) ^b
T_{eff} [K]	5460 ^c , 5600 ^d	5500 ± 100
T_{spot} [K]	3600 ± 400 ^c 3700 ± 150 ^d	3600 ^m ...
$v \sin i$ [km s^{-1}]	50 ^e	51 ± 0.5
P_{orb} [days]	1.947227 (8) ^c	1.947232 ± 0.000004
P_{phot} [days]	1.945 ^f 1.9527 ^g 1.952717 (31) ^h	1.95272 ± 0.00003
M_V [mag]	2.75 ⁱ	3.20 ± 0.12
L_1, L_2 [L_{\odot}]	–	$4.60 \pm 0.35, (0.01-0.02)$ ^b
R_1, R_2 [R_{\odot}]	≥ 1.9 ⁱ	$2.37 \pm 0.12, (0.3)$ ^b
M_1, M_2 [M_{\odot}]	$\geq 1.4, 0.53-1.3$ ⁱ	$1.09 \pm 0.05, 0.23 \pm 0.04$
Inclination [$^{\circ}$]	$34 \leq i \leq 58$ ⁱ	56.0 ± 4.5
Parallax [mas]	17.80 ± 0.97 ^j	–
Distance [pc]	56.2 ± 3.1 ^j	–
Ang. diam. [mas]	$0.4-0.6$ ^k	0.3921 ± 0.0006
Age [Gyr]	–	6.15 ± 0.50

^a ... Cutispoto (1995)

^b ... according to $M_2 = 0.23 M_{\odot}$ from §4.5 and the spectral type-luminosity tables in Schmidt-Kaler (1982).

^c ... Strassmeier (1990)

^d ... O’Neal et al. (1998)

^e ... Fekel et al. (1986)

^f ... Hall et al. (1987)

^g ... Olah et al. (2000, 2002)

^h ... Strassmeier et al. (1997)

ⁱ ... Fekel et al. (1987)

^j ... ESA (1997)

^k ... Wittkowski et al. (2002)

^m ... see paper II of this series

to the projected rotational velocity and provides better accuracy than any other method, as it takes into account the line deformation due to spots. Tests with images of the $\lambda 6393$, $\lambda 6411$ and $\lambda 6439$ line using the Doppler imaging codes TEMP MAP and DOTS lead to a value of $51.0 \pm 0.5 \text{ km s}^{-1}$. See paper II of this series.

The minimum stellar radius $R \sin i = (P_{\text{rot}} \cdot v \sin i) / 50.6$ with $P_{\text{rot}} = P_{\text{orb}} = 1.9472324 \pm 0.0000038$ is $1.963 \pm 0.019 R_{\odot}$.³ Obviously, EI Eri’s primary star is a subgiant rather than a dwarf, ruling out the luminosity class V suggested earlier by Abt (1986).

4.3 Luminosity and radius

The *Hipparcos* spacecraft measured a trigonometric parallax of 17.80 ± 0.97 milli-arcsec (ESA 1997), corresponding

³ Compare: For $P_{\text{rot}} = P_{\text{phot}} = 1.9527 \pm 0.0001$, we get $R \sin i = 1.968 \pm 0.019 R_{\odot}$. In paper III, we will address the different values of the photometric and orbital period.

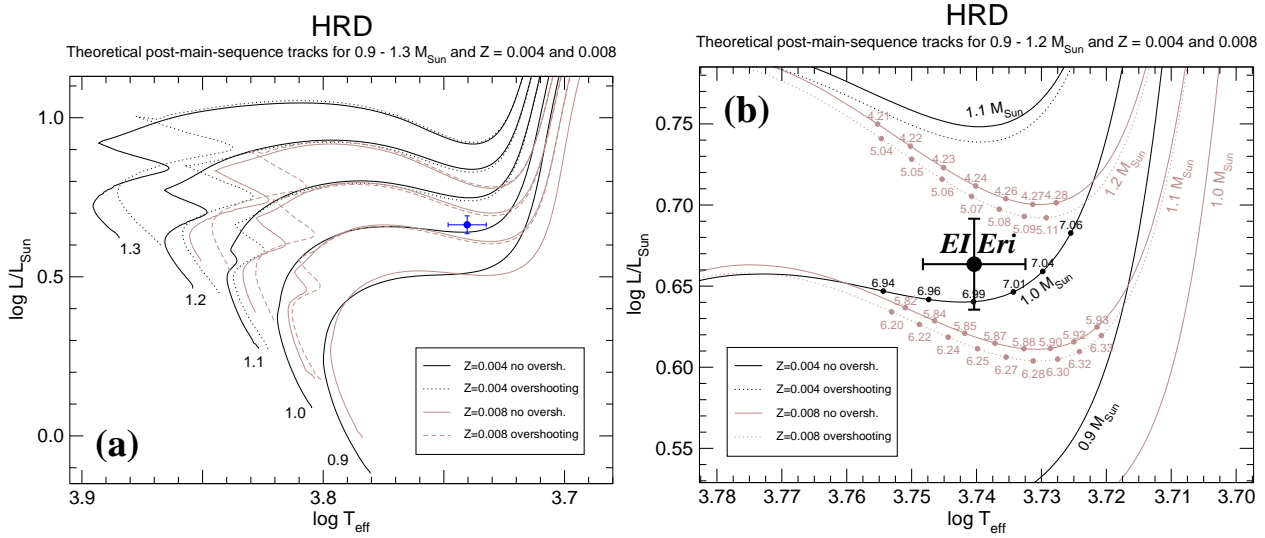


Fig. 4 (a) Evolutionary tracks for post-main-sequence stars from Pietrinferni et al. (2004) for masses of 0.9 – 1.3 M_{\odot} and for two different metallicities. The position of EI Eridani is marked at $\log T_{\text{eff}} = 3.740 \pm 0.008$ (5500 ± 100 K) and $\log L/L_{\odot} = 0.66 \pm 0.03$ ($4.6 \pm 0.3 L_{\odot}$). (b) shows the central range of (a) but adding age along the evolutionary tracks (the values are Gyr). For a metallicity of $Z = 0.006$, these tracks suggest a primary mass of $M_1 = 1.09 \pm 0.05 M_{\odot}$ and an age of 6.15 ± 0.50 Gyr.

to a distance of 56.2 ± 3.1 pc. The brightest (least-spotted) V magnitude of EI Eridani was observed on December 18, 2001, by the Vienna APTs and corresponds to $6^{\text{m}}949$. We adopt this as the least spotted V brightness. Combined with the distance, this gives $M_V = 3^{\text{m}}20 \pm 0.12$. According to Flower (1996), the bolometric correction for a subgiant with a temperature of 5500 ± 100 K is -0.139 ± 0.025 . Therefore, the bolometric magnitude is $3^{\text{m}}061 \pm 0.082$ (neglecting interstellar absorption as it is a nearby star). As we cannot adopt an external error for the maximum brightness the above error merely reflects the error of the parallax. However, if the brightest visual magnitude is smaller than $6^{\text{m}}9$, it does not affect the error of the stellar radius, but just the radius itself.

Adopting a solar bolometric magnitude of $4^{\text{m}}72$, we get the luminosity $L/L_{\odot} = 4.60 \pm 0.35$. Using $T_{\text{eff}} = 5500 \pm 100$ K, we obtain a stellar radius of $2.37 \pm 0.12 R_{\odot}$ from the Stefan-Boltzmann law (independent of the inclination) and consistent with the value of $R/R_{\odot} \geq 1.9$ from Fekel et al. (1987). This radius corresponds to an angular diameter of $\theta = 0.3921 \pm 0.0006$ mas, confirming the estimations from Wittkowski et al. (2002).

4.4 Orbital inclination

The analysis by Fekel et al. (1987) suggested an inclination between $15^{\circ} \leq i \leq 58^{\circ}$.⁴ We derive a primary mass of $M_1 = 1.09 \pm 0.05 M_{\odot}$ from T_{eff} and the parallax (see §4.5; both values are independent of the inclination). Using the

⁴ Note that Fekel et al. (1987) accidentally used $f(M) = 0.041$ instead of 0.0041 as listed in their paper. Accordingly, the values in their Table V are wrong. The correct inclination limits using their data values should read $15^{\circ} \leq i \leq 58^{\circ}$ instead of $34^{\circ} \leq i \leq 58^{\circ}$.

observed mass function $f(M) = 0.00391 \pm 0.00010$ (see Table 5), we achieve a minimum mass for the secondary (assuming $i = 90^{\circ}$) of $M_2 \geq 0.184 \pm 0.008 M_{\odot}$. This gives a maximum mass ratio of $M_1/M_2 \leq 5.91 \pm 0.25$ and an $a \sin i \leq 4.97 \pm 0.25 \cdot 10^6$ km. Because EI Eridani shows no eclipses (i.e., $R_1 + R_2 < a \cos i$), we can use our maximum value for $a \sin i$ and the radius R_1 and achieve maximum values for the orbital inclination: $i \leq 70^{\circ}9 \pm 2^{\circ}0$ for $R_2 = 0.1 R_{\odot}$, $i \leq 69^{\circ}5 \pm 1^{\circ}9$ for $R_2 = 0.3 R_{\odot}$, $i \leq 68^{\circ}1 \pm 1^{\circ}9$ for $R_2 = 0.5 R_{\odot}$ or $i \leq 66^{\circ}7 \pm 1^{\circ}9$ for $R_2 = 0.7 R_{\odot}$. Using $\sin i = (P_{\text{rot}} \cdot v \sin i) / (50.6 \cdot R/R_{\odot})$ and taking $P_{\text{rot}} = P_{\text{orb}}$, we obtain $i = 56.0 \pm 4.5^{\circ}$ in agreement with any of the above secondary radii. Assuming the orbital and the stellar rotational axis to be perpendicular, we adopt this as our final inclination value.

4.5 Mass and evolutionary status

Fekel et al. (1987) estimated $1.4 \leq M_1/M_{\odot} \leq 1.8$ for the primary and an upper limit for the secondary (for $i = 90^{\circ}$) of $1.0 - 1.3 M_1/M_{\odot}$. They suggested the secondary to be a late K or early M dwarf (since no evidence for a hot white dwarf companion is seen in the ultraviolet).

With the relatively precise luminosity from §4.3 and the effective temperature from §4.1, we can compare the position of EI Eridani's primary in the H-R diagram with theoretical evolutionary tracks. We use the scaled solar models from Pietrinferni et al. (2004). As argued in paper II, we assume abundances to be around -0.50 dex below solar, corresponding to a metallicity value of $Z = 0.006$. The closest models by Pietrinferni et al. (2004) have $Z = 0.004$ and 0.008 and are displayed in Fig. 4. The former corre-

sponds to a mass of $1.02 M_{\odot}$ and an age of 7.0 Gyr, the latter requires interpolation between the 1.1 and 1.2 solar-mass cases and results in $1.15 M_{\odot}$ and 5.0 Gyr (with overshooting) and $1.16 M_{\odot}$ and 5.6 Gyr (without overshooting).⁵ Interpolating both cases results in values of $1.09 \pm 0.05 M_{\odot}$ and 6.15 ± 0.50 Gyr. Comparing these results with the findings of Nordström et al. (2004), we see that mass is in excellent agreement with their value of $1.10^{+0.10}_{-0.12} M_{\odot}$ while age is well within the error bars of $5.5^{+1.2}_{-1.1}$ Gyr. Demircan et al. (2006), using old orbital data, give a total mass of $1.18 M_{\odot}$ and an age of 9.16 Gyr.

With the mass function $f(M) = (M_2 \sin i)^3 / (M_1 + M_2)^2 = 0.00391$ (see Table 3) and $i = 56^{\circ}0 \pm 4^{\circ}5$ (see §4.4), the primary mass of $1.09 \pm 0.05 M_{\odot}$ requires the mass of the secondary to be $0.228 \pm 0.044 M_{\odot}$ corresponding to $K_2 = 128 \pm 25 \text{ km s}^{-1}$ and $a_2 \sin i = 3.4 \pm 0.7 \cdot 10^6 \text{ km}$.

From the combined mass for the binary system ($M_1 + M_2$) of $1.32 \pm 0.07 M_{\odot}$, we can incorporate the mass function for the proposed binary/tertiary system (see §3.2) and repeat the above evaluation in order to estimate the tertiary mass M_3 . A period of 6700 ± 500 days yields (for the circular orbit): $M_3 = 0.7 \pm 0.6 M_{\odot}$ corresponding to $K_3 = 8 \pm 7 \text{ km s}^{-1}$ and $a_3 \sin i = 7 \pm 7 \cdot 10^8 \text{ km}$ (again for $i = 56^{\circ}0 \pm 4^{\circ}5$) with a being $9 \pm 6 \text{ AU}$ (corresponding to an angular separation from the binary of 0.3 arc sec). The large errors are mainly due to the large error in the mass function of the binary-tertiary orbit which itself is mainly due to the large error in $K_{1-2} = 4 \pm 1 \text{ km s}^{-1}$, the half-amplitude of the barycenter variation. The appropriate values for the eccentric orbit are $M_3 = 1.1 \pm 1.7 M_{\odot}$, $K_3 = 7 \pm 11 \text{ km s}^{-1}$, $a_3 \sin i = 6 \pm 10 \cdot 10^8 \text{ km}$ and $a = 9 \pm 8 \text{ AU}$.

4.6 Roche lobe and gravity

The Roche-lobe radius is determined from the semi-major orbital axis and the mass ratio. Assuming $M_1/M_2 = 4.77 \pm 0.05 M_{\odot}$ and $a \sin i = a_1 \sin i + a_2 \sin i = 4.145 \pm 0.725 \cdot 10^6 \text{ km}$, we can, using the formula from Eggleton (1983), calculate the Roche-lobe radii $R_{L,1} \sin i = 3.08 \pm 0.52 R_{\odot}$ and $R_{L,2} \sin i = 1.52 \pm 0.26 R_{\odot}$. Using $i = 56^{\circ}0 \pm 4^{\circ}5$, this translates to $R_{L,1} = 3.71 \pm 0.62 R_{\odot}$ and $R_{L,2} = 1.83 \pm 0.32 R_{\odot}$ for the primary and the secondary, respectively. This means that the primary fills $\approx 64 \pm 12\%$ of its Roche lobe but is still significantly detached from its inner critical equipotential surface. The secondary with assumed $R_2 \approx 0.3 R_{\odot}$ (for a M4-5 v; Schmidt-Kaler 1982) fills just 20% of its Roche lobe. Figure 5 shows a graphical view of the binary system. Shown are the location of the stellar surfaces and the inner and outer critical equipotentials as obtained with the program BinaryMaker (Bradstreet 1993).

O’Neal et al. (1996) list a gravity of $\log g \approx 3.8$ consistent with $\log g = 3.75$ used by Hackman et al. (1991). Randich et al. (1993) determined a $\log g$ of 4.1 using spectrum synthesis analysis. Gray (1992) lists a $\log g$ of 4.46

⁵ For $Z = 0.004$ and $M = 1.0 M_{\odot}$, only canonical models without overshooting are available.

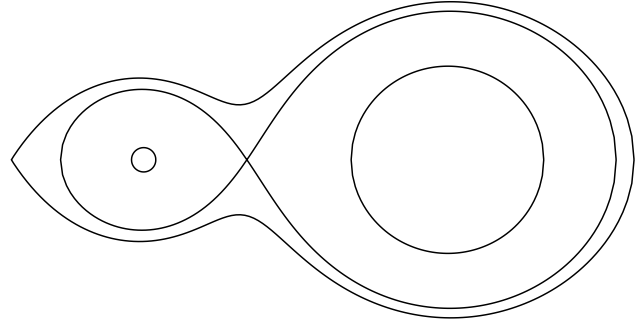


Fig. 5 Critical Roche equipotentials of the EI Eri system. The inner circles are the stellar surfaces, the other lines denote the inner and outer critical equipotentials, respectively. The G5 IV primary fills $\approx 64\%$ of its Roche lobe and is practically spherical in shape.

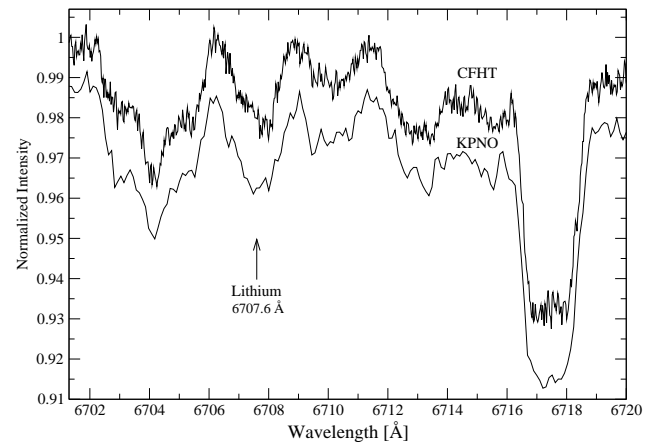


Fig. 6 Lithium spectra from CFHT and KPNO. The KPNO spectrum is shifted by -0.01 in intensity for better viewing. Signal-to-noise is $\approx 550/330$ (CFHT/KPNO), dispersion $0.027/0.103 \text{ Å}$, integration time $10/60 \text{ min}$.

for a G5 dwarf (V) and 3.3 for a G5 giant (III). Using the mass and radius of the primary from the previous analysis and applying the relation $g = GM/R^2$, where G is the gravitational constant, we can directly calculate $\log g$ to 3.73 ± 0.07 , in good agreement with previous claims.

4.7 Lithium abundance

Measurements of two spectra in the lithium region (one from CF96 and one from a CFHT observing run in October 1997; see Fig. 6) give an equivalent width of $40 \pm 5 \text{ mÅ}$ in good agreement with the value obtained by Fekel et al. (1987) of 36 mÅ . Comparing this to theoretical curves of growth from Pavlenko & Magazzu (1996), both LTE and non-LTE, we derive a lithium abundance of $\log n(\text{Li}) = 2.0$ for $T_{\text{eff}} = 5500 \text{ K}$ and $\log g = 3.5\text{--}4.5$. If the equivalent width is reduced to 25 mÅ to account for the Fe and V blends, the abundance is still $\log n(\text{Li}) = 1.75$. Randich et al. (1993) estimate $\log n(\text{Li}) = 1.8$ using spectrum synthesis analysis.

5 Summary

The following results were obtained:

- Improved orbital parameters were determined with HJD = $2,448,054.7109 + 1.9472324 \times E$, $\gamma = 21.6 \text{ km s}^{-1}$, $K_1 = 26.8 \text{ km s}^{-1}$. The barycenter velocity γ exhibits variations of about 8 km s^{-1} that are possibly cyclic. We interpret these variations due to a third stellar component and suggest a possible orbital solutions for the tertiary with a period of around 6700 days (19 years) and an amplitude of $4 - 6 \text{ km s}^{-1}$. An instrumental origin cannot be definitely ruled out. However, a thorough investigation of the orbit solutions of the individual observing runs and their radial velocity standard stars confirmed its reality in our data. The proposed period is also supported by the smaller $O-C$ radial velocity residuals. The third component would thereby surround the known binary system in a wide orbit. Corresponding values for the tertiary mass and the orbital parameters of the binary–tertiary system are quoted (Tab 4). However, its plausibility cannot be asserted unless a recurrence is observed or higher-quality RV measurements are available.
- From the *Hipparcos* parallax, we obtain a luminosity of $4.60 \pm 0.35 L_{\odot}$ and a radius of $2.37 \pm 0.12 R_{\odot}$, independent from the inclination.
- With our new parameters and by using evolutionary tracks from Pietrinferni et al. (2004), we locate the position of the primary in the HR diagram and determine its mass to $1.09 \pm 0.05 M_{\odot}$ and an age of $6.15 \pm 0.50 \text{ Gyr}$.
- The inclination is found to be $i = 56.0 \pm 4.5^{\circ}$.
- Using the observed mass function of the inner binary and assuming $i_{\text{orb}} \equiv i_*$, we derive the mass of the unseen secondary: $M_2 = 0.23 \pm 0.04 M_{\odot}$ corresponding to an absolute magnitude of $M_V \approx 12 \pm 1$ (Baraffe et al. 1998).

Acknowledgements. We are very grateful to the Deutsche Forschungsgemeinschaft for grant STR 645/1, for the Hungarian-German Intergovernmental Grant D21/01, and for the Hungarian Research Grant OTKA T-48961. Special thanks go to János Bartus for his support and computer assistance, to Frank Fekel for valuable discussions about the orbital solution, and to Johanna Jurcsik for help with the orbital period. This research project made extended use of the SIMBAD database, operated at CDS, Strasbourg, France. The orbit program by Barker and the utility `BinaryMaker` by David Bradstreet were used for this paper.

References

- Abt, H. A.: 1986, *ApJ* 309, 260
 Alonso, A., Arribas, S., Martinez-Roger, C.: 1996, *A&A* 313, 873
 Baraffe, I., Chabrier, G., Allard, F., Hauschildt, P. H.: 1998, *A&A* 337, 403
 Barker, E. S., Evans, D. S., Laing, J. D.: 1967, *Royal Greenwich Observatory Bulletin* 130, 355
 Bidelman, W. P., MacConnell, D. J.: 1973, *AJ* 78, 687
 Bradstreet, D. H.: 1993, *The Binary Maker manual*
 Cardini, D.: 2005, *A&A* 430, 303
 Chochol, D., Pribulla, T., Teodorani, M., Errico, L., Vittone, A. A., Milano, L., Barone, F.: 1998, *A&A* 340, 415
 Cutispoto, G.: 1995, *A&AS* 111, 507
 Demircan, O., Eker, Z., Karataş, Y., Bilir, S.: 2006, *MNRAS* 366, 1511
 Donati, J.-F., Semel, M., Carter, B. D., Rees, D. E., Collier Cameron, A.: 1997, *MNRAS* 291, 658
 Duemmler, R., Aarum, V.: 2001, *A&A* 370, 974
 Eggleton, P. P.: 1983, *ApJ* 268, 368
 ESA: 1997, *The Hipparcos and Tycho Catalogues, ESA SP-1200*
 Fekel, F. C.: 1980, In *First Cambridge Workshop on Cool Stars, Stellar Systems, and the Sun* volume 1, 133
 Fekel, F. C., Hall, D. S., Henry, G. W., Landis, H. J., Renner, T. R.: 1982, *IBVS* 2110, 1
 Fekel, F. C., Moffett, T. J., Henry, G. W.: 1986, *ApJS* 60, 551
 Fekel, F. C., Quigley, R., Gillies, K., Africano, J. L.: 1987, *AJ* 94, 726
 Fekel, F. C., Strassmeier, K. G., Weber, M., Washuettl, A.: 1999, *A&AS* 137, 369
 Fernandez-Figueroa, M. J., Montes, D., de Castro, E., Cornide, M.: 1994, *ApJS* 90, 433
 Fitzpatrick, M. J.: 1993, In Hanisch, R. J., Brissenden, R. J. V., Barnes, J., editors, *Astronomical Data Analysis Software and Systems II* volume 52 of *Astronomical Society of the Pacific Conference Series*, 472
 Flower, P. J.: 1996, *ApJ* 469, 355
 García-Sánchez, J., Paredes, J. M., Ribó, M.: 2003, *A&A* 403, 613
 Granzer, T., Reegen, P., Strassmeier, K. G.: 2001, *AN* 322, 325
 Gray, D. F.: 1992, *The observation and analysis of stellar photospheres*. Cambridge Astrophysics Series, Cambridge: Cambridge University Press, 2nd ed.
 Gunn, A. G., Hall, J. C., Lockwood, G. W., Doyle, J. G.: 1996, *A&A* 305, 146
 Hackman, T., Piskunov, N. E., Poutanen, M., Strassmeier, K. G., Tuominen, I.: 1991, In Tuominen, I., Moss, D., Rüdiger, G., editors, *IAU Colloq. 130: The Sun and Cool Stars. Activity, Magnetism, Dynamos* volume 380 of *Lecture Notes in Physics*, Berlin Springer Verlag, 321
 Hall, D. S., Osborn, S. A. G., Seufert, E. R., Boyd, L. J., Genet, R. M., Fried, R. E.: 1987, *AJ* 94, 723
 Harlan, E. A.: 1974, *AJ* 79, 682
 Hatzes, A. P., Vogt, S. S.: 1992, *MNRAS* 258, 387
 Hearnshaw, J.: 1979, In *IAU Colloq. 46: Changing Trends in Variable Star Research*, 371
 Kurucz, R. L.: 1993, *ATLAS-9 CD CD ROM No. 13*
 Lucy, L. B., Sweeney, M. A.: 1971, *AJ* 76, 544
 Nordström, B., Mayor, M., Andersen, J., Holmberg, J., Pont, F., Jørgensen, B. R., Olsen, E. H., et al.: 2004, *A&A* 418, 989
 Oláh, K., Strassmeier, K. G.: 2002, *AN* 323, 361
 O’Neal, D., Neff, J. E., Saar, S. H.: 1998, *ApJ* 507, 919
 O’Neal, D., Saar, S. H., Neff, J. E.: 1996, *ApJ* 463, 766
 Osten, R. A., Brown, A., Wood, B. E., Brady, P.: 2002, *ApJS* 138, 99
 Pallavicini, R., Randich, S., Giampapa, M. S.: 1992, *A&A* 253, 185
 Pavlenko, Y. V., Magazzu, A.: 1996, *A&A* 311, 961
 Pearce, J. A.: 1955, *Trans. IAU* 9, 441
 Pietrinferni, A., Cassisi, S., Salaris, M., Castelli, F.: 2004, *ApJ* 612, 168
 Randich, S., Gratton, R., Pallavicini, R.: 1993, *A&A* 273, 194

- Rice, J. B.: 2002, AN 323, 220
- Rodono, M., Cutispoto, G.: 1992, A&AS 95, 55
- Scarfe, C. D., Batten, A. H., Fletcher, J. M.: 1990, Publ. Dom. Astrophys. Obs. 18, 21
- Schmidt-Kaler, T.: 1982, In Schaifers, K., Voigt, H. H., editors, *Landolt-Börnstein* volume 2b. Springer Verlag Berlin Heidelberg New York
- Smith, M. A., Giampapa, M. S.: 1987, In Linsky, J. L., Stencel, R. E., editors, *Cool Stars, Stellar Systems and the Sun* volume 291 of *Lecture Notes in Physics, Berlin Springer Verlag*, 477
- Smith, M. A., Jaksha, B. B.: 1984, In Baliunas, S. L., Hartmann, L., editors, *Cool Stars, Stellar Systems, and the Sun* volume 193 of *Lecture Notes in Physics, Berlin Springer Verlag*, 182
- Smith, S. E., Bopp, B. W.: 1982, Astrophys. Lett. 22, 127
- Strassmeier, K. G.: 1990, ApJ 348, 682
- Strassmeier, K. G., Bartus, J., Cutispoto, G., Rodonó, M.: 1997, A&AS 125, 11
- Strassmeier, K. G., Boyd, L. J., Epand, D. H., Granzer, T.: 1997, PASP 109, 697
- Strassmeier, K. G., Fekel, F. C., Bopp, B. W., Dempsey, R. C., Henry, G. W.: 1990, ApJS 72, 191
- Strassmeier, K. G., Hall, D. S., Boyd, L. J., Genet, R. M.: 1989, ApJS 69, 141
- Strassmeier, K. G., Rice, J. B., Wehlau, W. H., Vogt, S. S., Hatzes, A. P., Tuominen, I., Hackman, T., Poutanen, M., Piskunov, N. E.: 1991, A&A 247, 130
- Washuettl, A., Kővári, Zs., Foing, B. H., Oláh, K., Vida, K., Bartus, J., Weber, M., et al.: 2009a, A&A, Submitted (Paper III)
- Washuettl, A., Strassmeier, K. G., Collier-Cameron, A.: 2001, In Garcia Lopez, R. J., Rebolo, R., Zapaterio Osorio, M. R., editors, *11th Cambridge Workshop on Cool Stars, Stellar Systems and the Sun* volume 223 of *Astronomical Society of the Pacific Conference Series*, 1308
- Washuettl, A., Strassmeier, K. G., Weber, M.: 2009b, AN, Submitted (Paper II)
- Weber, M., Strassmeier, K. G.: 1998, A&A 330, 1029
- Wilson, R. E.: 1953, General Catalogue of Stellar Radial Velocities; Carnegie Institute Washington D.C. Publication
- Wittkowski, M., Schöller, M., Hubrig, S., Posselt, B., von der Lüche, O.: 2002, AN 323, 241
- Zboril, M., Oliveira, J. M., Messina, S., Djurašević, G., Amado, P. J.: 2005, Contributions of the Astronomical Observatory Skalnaté Pleso 35, 23
- Zuckerman, B., Webb, R. A., Becklin, E. E., McLean, I. S., Malkan, M. A.: 1997, AJ 114, 805

NSO, Nov 16 – Dec 22, 1988

A Observing logs (Online material)

Observing logs for all data used in this investigation, the ones from our own observing runs as well as the ones from the literature, are specified in the following tables. The tables list the Heliocentric Julian Date (HJD) at the midpoint of an observation, the exposure time (combined exposure time in case of combined images; actually, CCD dark time is used), the signal-to-noise ratio as estimated using IRAF's `splot`, the phase, the heliocentric radial velocity v_r in km s^{-1} , and the error of the radial velocity measurement σ_{v_r} in km s^{-1} ("DI" means that v_r was estimated by means of Doppler imaging, and no σ_{v_r} can be given). For the MUSICOS 98 data, the observing site is listed as well, and the HJD had to be abbreviated (24511+). For the data from the literature, HJD (244+), phase, v_r , the used instrument, and a reference code is given.

HJD	t_{exp} [s]	S/N	phase	v_r [km s ⁻¹]	σ_{v_r}
2447481.85877934	3600	280	0.8121	22.92	(DI)
2447482.72595936	2400	240	0.2575	11.59	(DI)
2447485.78022403	3000	270	0.8260	24.96	(DI)
2447485.91420547	4500	270	0.8948	35.20	(DI)
2447486.78984068	2400	270	0.3445	-1.94	(DI)
2447486.92332404	2400	290	0.4130	-10.62	(DI)
2447492.77544820	2400	280	0.4184	-10.40	(DI)
2447493.80873462	2400	270	0.9490	38.34	(DI)
2447494.86839555	1500	250	0.4932	-14.11	(DI)
2447508.90138814	1800	290	0.6999	3.99	(DI)
2447509.78106126	2100	270	0.1516	30.67	(DI)
2447509.80592715	1800	280	0.1644	29.19	(DI)
2447511.78858361	2400	280	0.1826	24.80	(DI)
2447511.93134400	2509	200	0.2559	13.26	(DI)
2447513.77129171	1800	230	0.2008	20.90	(DI)
2447513.92290565	2100	200	0.2787	8.24	(DI)
2447517.92410247	3900	250	0.3335	-0.36	(DI)

NSO, Jan 12 – Jan 31, 1989

HJD	t_{exp}	S/N	phase	v_r	σ_{v_r}
2447538.81751973	3600	370	0.0633	46.11	(DI)
2447545.69961784	1815	340	0.5976	-6.03	(DI)
2447546.67373727	1680	330	0.0978	42.21	(DI)
2447549.68456430	1800	270	0.6440	-1.07	(DI)
2447556.69637278	2700	340	0.2449	19.06	(DI)
2447557.69618472	2400	380	0.7584	17.01	(DI)

NSO, Nov 9, 1989, – Jan 24, 1990

HJD	t_{exp}	S/N	phase	v_r	σ_{v_r}
2447839.90839991	2700	310	0.6883	–	–
2447840.69110908	2400	260	0.0903	–	–
2447841.92716837	2400	280	0.7250	–	–
2447864.96392067	2100	240	0.5556	–	–
2447865.94967414	2400	320	0.0618	–	–
2447878.94827398	3000	150	0.7372	–	–
2447898.78161089	2400	200	0.9226	–	–
2447899.77544479	2100	200	0.4330	–	–
2447900.77487947	1800	310	0.9463	–	–
2447900.80027108	2100	280	0.9593	–	–
2447901.64796707	1200	280	0.3946	–	–
2447901.66231884	1200	240	0.4020	–	–
2447902.73509105	1200	240	0.9529	–	–
2447902.74944197	1200	250	0.9603	–	–
2447903.72759042	1200	230	0.4626	–	–
2447903.74192943	1200	240	0.4700	–	–
2447912.81237266	1800	210	0.1281	–	–
2447915.68691188	1800	240	0.6043	–	–
2447925.76718365	2400	200	0.7810	–	–
2447925.81426603	2700	230	0.8052	–	–

NSO, Oct 23 – Dec 2, 1990

HJD	t_{exp}	S/N	phase	v_r	σ_{v_r}
2448187.90907048	2100	280	0.4038	1.51	2.17
2448188.88383156	1800	350	0.9044	44.40	2.31
2448189.80971259	1800	280	0.3799	8.86	5.90
2448199.04278572	2280	320	0.1216	–	–
2448200.03172236	3600	240	0.6294	4.80	1.73
2448204.01902843	4200	370	0.6771	10.62	1.86
2448211.90627687	1800	330	0.7276	18.67	1.71
2448214.92815164	2400	310	0.2795	17.85	2.05
2448224.00487253	3300	300	0.9408	49.40	2.16
2448227.84227865	3000	340	0.9115	45.78	1.58

NSO, Jan 15 – Jan 31 / Mar 8, 1991

HJD	t_{exp}	S/N	phase	v_r	σ_{v_r}
2448271.80021084	2700	300	0.4861	-3.45	1.82
2448272.87407843	3000	230	0.0376	48.61	3.50
2448274.79259064	2700	360	0.0228	49.77	1.64
2448284.81303141	2700	390	0.1688	36.82	2.16
2448286.79004258	4800	390	0.1841	34.83	1.70
2448287.78336189	1800	360	0.6942	14.03	1.66
2448323.74119835	946	110	0.1603	37.02	1.98
2448330.66309608	3900	350	0.7151	17.80	1.98
2448333.67863402	4200	280	0.2637	21.20	1.61

NSO, Jan 9 – Feb 5, 1992

HJD	t_{exp}	S/N	phase	v_r	σ_{v_r}
2448536.84220564	2400	300	0.5982	2.94	1.89
2448571.87915138	2400	300	0.5915	1.38	2.01
2448572.73822549	2100	250	0.0326	50.73	1.69
2448573.96871468	2100	300	0.6645	10.30	1.62
2448583.76049664	2700	250	0.6931	12.33	1.67
2448583.78916548	1500	300	0.7078	15.78	1.58
2448584.73695026	2400	350	0.1946 (32.59)	(1.54)	
2448585.90944273	1800	300	0.7967	32.25	2.12
2448586.88967786	1800	300	0.3001	15.67	1.84
2448587.69108233	1800	300	0.7117	21.44	1.98
2448594.77324122	3600	350	0.3487	8.40	2.08
2448597.73887879	2400	300	0.8717	42.13	1.96
2448598.95181001	3900	250	0.4946	-2.56	2.02

2448630.80189166	4500	300	0.8512	39.14	1.81
2448631.73144606	4200	375	0.3285	9.93	2.00
2448635.74885926	4200	300	0.3917	2.60	1.96
2448644.72706482	2400	375	0.0025	51.21	1.93
2448645.75364952	2700	350	0.5296	-2.93	1.79
2448646.79759322	2700	325	0.0658	48.68	2.17
2448647.72925336	4500	350	0.5442	-3.29	2.15
2448657.74044939	3300	325	0.6854	14.11	2.59

NSO, Oct 14 – Dec 1, 1992

HJD	t_{exp}	S/N	phase	v_r	σ_{v_r}
2448909.81574167	3300	350	0.1386	38.89	1.80
2448910.82189280	2700	320	0.6553	9.57	2.53
2448911.76449788	2100	220	0.1393	39.80	2.90
2448919.01267057	2520	280	0.8616	41.80	2.41
2448919.80544506	2400	250	0.2688	19.80	1.84
2448921.92832595	1920	320	0.3590	5.41	1.47

2448932.98758668	3000	300	0.0384	49.89	6.25
2448933.85932839	1800	350	0.4861	-3.52	1.40
2448934.97814509	2400	280	0.0607	49.12	1.87
2448935.97845108	4200	360	0.5744	2.31	1.53
2448947.99180786	4500	140	0.7439	24.23	1.72
2448954.93973981	3300	320	0.3120	10.72	1.07
2448955.91696006	2961	130	0.8138	35.42	1.97
2448957.74816912	3300	380	0.7542	26.90	1.76

NSO, January 29 – April 2, 1993

HJD	t_{exp}	S/N	phase	v_r	σ_{v_r}
2447866.97849159	2400		0.5901	–	–
2447875.77605125	1800		0.1081	–	–
2448958.85377396	3000		0.3220	–	–
2449016.74254290	4200	300	0.0508	48.96	1.53
2449030.68296247	2700	350	0.2098	30.22	1.63
2449030.70657099	1200	250	0.2220	27.71	1.93
2449066.66889489	4200	250	0.6904	14.14	1.54
2449078.66783958	1452	100	0.8525	43.72	4.22
2449079.66842867	2023	140	0.3663	3.87	2.57

NSO, October 20 – November 4, 1993

HJD	t_{exp}	S/N	phase	v_r	σ_{v_r}
2449280.92690392	2100	350	0.7225	19.75	2.35
2449281.99038834	2100	300	0.2686	20.99	1.70
2449282.81566634	3000	380	0.6924	16.17	1.60
2449283.03415929	1500	320	0.8046	33.03	1.57
2449291.85534333	1800	320	0.3348	10.40	1.15
2449293.00654551	1656	280	0.9260	48.62	1.53
2449294.82520519	1500	350	0.8599	40.48	1.41
2449295.85622598	1500	320	0.3894	3.78	1.20

NSO, November 11 – December 9, 1993

HJD	t_{exp}	S/N	phase	v_r	σ_{v_r}
2449302.86739868	1800	380	0.9900	51.32	1.83
2449326.88055564	1500	380	0.3219	12.57	2.19
2449327.67699497	1200	320	0.7309	21.65	1.49
2449328.74862305	900	280	0.2813	18.86	1.59
2449329.72085393	1500	320	0.7806	29.18	1.32
2449330.75974826	3000	220	0.3141	10.62	1.51
2449330.80034305	3000	220	0.3349	9.50	1.75

NSO, January 30 – February 1, 1994

HJD	t_{exp}	S/N	phase	v_r	σ_{v_r}
2449382.70823625	1800	240	0.9922	51.12	1.86
2449382.72958862	1800	220	0.0032	51.86	1.70
2449383.63808861	1200	280	0.4697	-2.04	1.05
2449383.65247397	1200	330	0.4771	-1.96	1.40
2449384.63884888	1800	320	0.9837	50.72	1.97
2449384.66018966	1800	300	0.9946	50.92	1.70

NSO, November 11 – December 9, 1993

HJD	t_{exp}	S/N	phase	v_r	σ_{v_r}
2449416.61073607	1500	300	0.4028	4.30	1.63
2449417.64027834	1800	230	0.9315	49.07	1.50
2449418.62555397	2700	270	0.4375	0.20	2.07
2449427.62140418	1800	180	0.0573	49.98	1.16
2449427.64274509	1800	160	0.0683	49.50	1.61
2449427.66438765	1800	150	0.0794	48.53	1.81
2449427.68571774	1800	150	0.0904	47.35	3.36
2449428.60637301	1800	300	0.5632	-0.07	1.70
2449429.60576848	1800	180	0.0764	47.06	1.54
2449429.62775173	1800	250	0.0877	46.26	1.76
2449429.64908147	1800	250	0.0987	45.24	1.83
2449429.67041157	1800	250	0.1096	43.68	2.19
2449429.68829901	1200	180	0.1188	42.39	2.37
2449430.66364978	1630	100	0.6197	4.68	2.62
2449439.60910082	1500	280	0.2136	31.55	1.40
2449440.64563261	2700	320	0.7459	23.73	1.56
2449440.66718426	510	60	0.7570	25.62	3.94
2449442.60931421	1200	250	0.7544	26.23	2.52
2449442.62722388	1800	320	0.7636	27.38	1.55
2449442.64896526	1800	280	0.7747	29.83	1.78
2449443.59744365	900	230	0.2618	25.33	1.62

NSO, October 18 – October 31, 1994

HJD	t_{exp}	S/N	phase	v_r	σ_{v_r}
2449643.94619938	2700	250	0.1508	39.03	1.70
2449644.73987058	2700	160	0.5584	-0.98	2.37
2449644.77161854	2700	190	0.5747	0.09	2.58
2449644.97355043	2700	230	0.6784	14.64	2.57
2449645.71373397	2700	60	0.0585	47.97	3.02
2449645.74549183	2700	140	0.0748	46.68	2.45
2449645.77770689	2700	180	0.0914	45.39	2.06
2449646.90943591	2700	230	0.6726	12.77	1.76
2449646.94642850	3600	270	0.6916	15.48	1.88
2449647.94902364	3600	150	0.2065	29.23	3.38
2449647.99254978	3600	150	0.2288	27.75	2.40
2449648.03095424	2520	240	0.2485	23.85	2.31
2449648.98419955	2700	180	0.7381	22.43	1.40
2449649.01596035	2700	220	0.7544	24.85	1.66
2449649.04090361	1410	170	0.7672	26.65	2.47
2449656.86531271	3600	250	0.7854	29.86	1.84

NSO, December 17, 1994 – January 3, 1995

HJD	t_{exp}	S/N	phase	v_r	σ_{v_r}
2449703.79438644	2700	250	0.8858	44.89	1.88
2449703.82614415	2700	230	0.9021	45.74	1.74
2449704.58565054	1800	220	0.2922	17.56	1.85
2449704.60699218	1800	210	0.3031	16.07	1.80
2449704.62835689	1800	180	0.3141	14.21	1.75
2449705.59374487	2700	280	0.8099	35.55	1.41
2449705.62551423	2700	280	0.8262	38.19	1.41
2449705.78176925	1800	300	0.9064	46.42	1.41
2449705.80311061	1800	320	0.9174	48.06	1.42
2449706.82943194	2700	340	0.4444	-0.87	1.44
2449707.59811282	3600	310	0.8392	39.82	1.72
2449708.74437943	1800	330	0.4279	0.53	1.47
2449715.81930526	2700	280	0.0612	49.33	1.49

2449715.85246988	2700	170	0.0782	48.26	1.70
2449717.78351050	2700	270	0.0699	48.78	1.77
2449717.81527916	2700	320	0.0862	47.84	1.42
2449717.84704816	2700	300	0.1025	46.33	1.64
2449718.60435442	2700	150	0.4915	-1.50	2.22
2449718.63653990	2700	220	0.5080	-1.01	1.24
2449720.82242596	1800	200	0.6305	7.35	2.42
2449720.84382622	1800	200	0.6415	9.00	1.73

NSO, February 17 – 20, 1995

HJD	t_{exp}	S/N	phase	v_r	σ_{v_r}
2449765.67120109	2700	100	0.6626	11.69	5.51
2449765.70260143	2700	110	0.6787	10.71	11.64
2449768.63353196	1800	80	0.1839	34.77	3.72
2449768.65450472	1800	70	0.1947	33.26	2.27
2449768.67594000	1800	70	0.2057	31.08	1.98

NSO, February 28 – March 28, 1995

HJD	t_{exp}	S/N	phase	v_r	σ_{v_r}
2449776.64514955	377	80	0.2983	18.69	4.60
2449787.61740737	2700	90	0.9331	46.40	2.24
2449787.64879368	2700	100	0.9492	47.24	3.63
2449791.64808752	2700	130	0.0030	49.53	2.82
2449791.67947504	2700	160	0.0191	49.56	3.18
2449799.64329404	3600	160	0.1089	44.23	2.67
2449800.63200616	2700	70	0.6167	5.99	5.68
2449800.66339303	2700	70	0.6328	9.19	7.10
2449802.63812302	2700	170	0.6469	9.02	3.56
2449802.66952217	2700	160	0.6631	11.74	2.89
2449804.62434905	2700	260	0.6670	10.16	2.89
2449804.65574755	2700	240	0.6831	12.08	5.45

NSO, October 1 – 2, 1995

HJD	t_{exp}	S/N	phase	v_r	σ_{v_r}
2449992.02679	2400	50	0.9074	43.78	7.19
2449992.84405	3600	60	0.3271	11.40	6.06
2449992.89221	3600	150	0.3518	8.25	4.77

NSO, November 7 – December 2, 1995

HJD	t_{exp}	S/N	phase	v_r	σ_{v_r}
2450029.03403	3600	220	0.9124	47.50	2.40
2450029.84153	3600	260	0.3271	13.59	4.46
2450031.97660	3600	360	0.4236	0.40	1.50
2450032.82948	3000	380	0.8616	40.93	3.72
2450039.89632	3600	400	0.4907	-0.87	2.41
2450040.82260	3600	320	0.9664	53.97	3.72
2450040.90672	2400	330	0.0096	55.43	4.15
2450041.87009	2700	300	0.5044	-1.25	2.50
2450042.80285	2700	300	0.9834	49.42	3.01
2450042.88547	2700	320	0.0258	52.19	3.20
2450043.65585	2700	250	0.4214	2.36	2.23
2450044.85677	2100	280	0.0382	51.24	4.95
2450051.89799	1800	320	0.6542	8.48	1.50
2450052.88745	1800	310	0.1623	36.68	3.20
2450053.80507	1800	330	0.6336	6.17	1.33

NSO, December 12 – 28, 1995						
HJD	t_{exp}	S/N	phase	v_r	σ_{v_r}	
2450063.93937	3600	400	0.8380	40.14	5.86	
2450065.87490	3600	360	0.8320	36.14	2.26	
2450066.86716	3600	340	0.3416	9.60	4.93	
2450078.88520	3600	320	0.5135	-2.43	5.57	
2450079.89740	3600	180	0.0333	52.65	2.34	

NSO, Nov 1, 1996 – Jan 8, 1997						
HJD	t_{exp}	S/N	phase	v_r	σ_{v_r}	
2450388.90290475	3600	150	0.7229	13.40	7.6	
2450390.99888385	3000	130	0.7992	24.88	8.1	
2450391.98128049	3600	150	0.3038	11.50	7.8	
2450392.96932388	2700	130	0.8112	21.84	7.7	
2450393.99213488	2700	160	0.3364	11.35	7.0	
2450394.68500721	3600	150	0.6923	9.09	7.3	
2450394.96069560	1200	160	0.8338	33.84	7.8	
2450395.68942407	1800	140	0.2081	24.67	6.9	
2450395.98469570	1200	160	0.3597	4.79	7.3	
2450396.72716891	3600	160	0.7410	19.95	6.8	
2450399.77645195	4351	140	0.3070	8.66	7.2	
2450400.88806165	3600	130	0.8778	37.02	7.9	
2450401.87706386	3600	140	0.3857	0.33	7.0	
2450404.71751004	3600	150	0.8444	31.27	7.4	
2450404.95373214	1260	120	0.9657	44.96	7.6	
2450405.93025135	1800	140	0.4672	-7.20	7.6	
2450406.79314622	900	140	0.9104	42.55	7.0	
2450406.92499244	900	150	0.9781	44.01	7.6	
2450408.75429680	1260	140	0.9175	43.61	8.0	
2450408.86176188	900	120	0.9727	47.67	8.6	
2450408.95522238	900	140	0.0207	47.40	7.7	
2450409.75060189	1800	130	0.4292	-3.87	7.3	
2450409.87995318	1800	140	0.4956	-7.74	7.4	
2450411.84548705	2700	140	0.5050	-5.61	7.2	
2450412.86152074	2700	150	0.0268	43.92	7.2	
2450414.75119559	2700	140	0.9972	45.59	8.4	
2450415.78868308	2700	140	0.5300	-4.54	7.4	
2450416.84316521	2700	140	0.0716	43.77	8.0	
2450417.87992018	3600	130	0.6040	-2.33	6.7	
2450418.86438290	1800	140	0.1096	36.45	8.9	
2450419.70589534	1800	140	0.5417	-4.57	7.6	
2450420.68467254	1800	140	0.0444	42.15	8.0	
2450421.80456207	1080	150	0.6195	-2.76	8.2	
2450422.79352103	1080	130	0.1274	34.40	8.5	
2450423.78074261	1260	130	0.6343	1.02	6.8	
2450424.90900056	1800	140	0.2138	21.38	8.4	
2450425.88593564	1800	150	0.7155	10.92	7.2	
2450426.89264277	1800	140	0.2325	19.08	8.6	
2450428.91439143	1800	130	0.2707	13.82	8.2	
2450429.87755393	1800	150	0.7654	18.65	8.0	
2450430.88667993	1800	150	0.2836	12.93	7.8	
2450431.71075924	1800	150	0.7068	10.53	6.9	
2450432.89437238	1800	150	0.3146	7.32	7.7	

2450435.73593090	2700	130	0.7739	21.00	7.0	
2450436.72737582	2700	140	0.2831	11.22	7.6	
2450437.78293088	1260	140	0.8252	27.44	7.2	
2450438.88091902	1800	140	0.3890	1.13	7.6	
2450440.72651416	1800	130	0.3368	6.08	5.9	
2450441.87574535	1260	140	0.9270	44.35	6.7	
2450446.65767851	2232	140	0.3828	-0.36	6.2	
2450447.83059191	900	130	0.9851	43.29	8.0	
2450448.70624150	900	140	0.4348	-6.85	6.8	
2450450.82337754	900	130	0.5221	-7.65	7.6	
2450451.83619104	1260	120	0.0422	43.62	7.4	
2450453.74258670	1676	100	0.0212	43.78	7.8	
2450454.82479083	2700	120	0.5770	-5.12	7.5	
2450456.83642216	3600	130	0.6101	-1.62	7.2	
2450457.76155057	1440	130	0.0852	40.43	8.2	

KPNO, Mar 4 – Mar 18, 1994						
HJD	t_{exp}	S/N	phase	v_r	σ_{v_r}	
2449416.61902162	1917	200	0.4071	-2.40	3.0	
2449417.61724752	3000	270	0.9197	43.65	4.4	
2449426.60346990	3000	300	0.5346	-7.75	3.4	

KPNO, Feb 22 – Mar 7, 1995						
HJD	t_{exp}	S/N	phase	v_r	σ_{v_r}	
2449770.60061516	3000	200	0.1941	28.79	4.7	
2449773.61609044	3000	200	0.7427	11.56	4.9	
2449774.59440811	2554	200	0.2451	19.73	6.6	
2449781.59376862	2204	180	0.8396	34.63	7.2	
2449783.61495233	2312	210	0.8776	39.89	7.2	

KPNO, Jan 10 – 24, 1996						
HJD	t_{exp}	S/N	phase	v_r	σ_{v_r}	
2450093.58895868	1800	310	0.0646	47.48	3.63	
2450093.72198162	3600	320	0.1329	39.57	3.20	
2450093.86983001	2429	330	0.2088	29.50	3.22	
2450094.58586781	3600	270	0.5765	-0.35	3.99	
2450094.75631891	3600	190	0.6641	9.93	4.10	
2450094.84253948	3600	280	0.7083	18.69	4.40	
2450095.59933732	3600	350	0.0970	45.06	2.25	
2450095.84999107	3600	360	0.2257	29.28	2.30	
2450096.58167400	3600	370	0.6015	1.03	3.63	
2450096.84057936	3600	360	0.7344	22.23	2.60	
2450098.58923565	3676	300	0.6324	5.23	2.35	
2450100.63909368	3600	240	0.6852	13.49	2.70	
2450100.83270193	3600	310	0.7846	30.55	2.48	
2450101.58188063	3600	220	0.1693	35.55	3.54	
2450101.72781877	3600	330	0.2443	22.79	2.05	
2450102.72229088	3600	270	0.7550	23.66	2.28	
2450103.72935395	3600	190	0.2722	18.63	1.83	
2450103.83519003	3600	210	0.3265	10.44	1.78	
2450106.60196237	2705	180	0.7474	22.37	2.39	
2450106.71444160	3600	250	0.8051	31.37	2.35	
2450106.83906083	3005	350	0.8692	39.50	2.49	
2450107.68453725	3600	190	0.3033	8.19	2.00	
2450107.77017848	3600	280	0.3473	2.75	2.01	
2450107.82899318	3600	220	0.3775	0.75	2.35	

KPNO, Dec 26, 1997 – Jan 14, 1998.

HJD	t_{exp}	S/N	phase	v_r	σ_{v_r}
2450809.58273645	3640	299	0.7627	20.68	2.2
2450809.72859092	5135	294	0.8376	32.50	1.9
2450809.86952719	5078	237	0.9100	42.79	2.0
2450810.58576035	3642	288	0.2778	14.96	2.0
2450810.68774591	4798	221	0.3302	6.80	2.2
2450810.82391309	4555	153	0.4001	-0.53	2.0
2450811.62176909	3672	188	0.8099	28.22	1.8
2450811.72285058	3642	198	0.8618	36.34	2.3
2450811.82025871	3639	232	0.9118	42.17	1.9
2450811.90381865	2727	201	0.9547	45.86	1.6
2450812.86269379	900	81	0.4471	-5.48	1.9
2450813.58682342	3643	312	0.8190	30.62	2.3
2450813.68721789	3642	372	0.8706	37.31	1.9
2450813.80771387	8085	389	0.9325	45.17	1.5
2450813.89197395	3642	333	0.9757	47.30	1.8
2450814.58051026	3640	348	0.3293	7.42	1.7
2450814.66755949	3641	383	0.3740	1.37	2.2
2450814.72819247	3445	376	0.4052	-1.22	1.9
2450814.81155554	3241	368	0.4480	-3.79	2.3
2450814.91346455	2300	107	0.5003	-8.52	2.1
2450815.58646849	3544	360	0.8459	34.89	2.2
2450815.68379471	3641	381	0.8959	40.47	2.2
2450815.79300152	3643	361	0.9520	44.52	2.2
2450815.85301531	900	184	0.9828	48.18	1.9
2450816.58303964	3642	319	0.3577	2.53	1.8
2450819.66147317	3643	313	0.9387	43.50	2.1
2450819.77794707	3641	323	0.9985	46.63	2.0
2450819.87733875	3641	280	0.0495	44.08	2.2
2450820.57320682	3643	328	0.4069	-3.37	1.7
2450820.68061358	3644	302	0.4620	-5.41	1.7
2450820.78112776	3642	334	0.5137	-6.18	1.6
2450820.87562960	3643	265	0.5622	-4.86	1.8
2450821.57235406	3643	332	0.9200	43.51	1.7
2450821.67462729	3643	361	0.9725	47.03	1.5
2450821.77773380	3643	363	0.0255	47.53	1.7
2450821.88964179	1830	91	0.0829	42.76	1.8
2450822.71209769	4820	308	0.5053	-7.25	2.0
2450822.81245542	3643	368	0.5568	-4.62	1.8
2450822.86863216	3641	325	0.5857	-2.93	2.1
2450823.78021880	3644	362	0.0538	45.33	2.0
2450825.62981148	3644	368	0.0037	46.19	1.9
2450825.71605559	3642	361	0.0480	44.99	1.8
2450825.78051100	3641	341	0.0811	43.04	2.1
2450825.86746150	3643	253	0.1257	38.20	1.6
2450826.58727787	3642	358	0.4954	-7.26	2.0
2450826.71078173	3641	374	0.5588	-5.73	2.1
2450826.77149497	3641	356	0.5900	-3.41	1.8
2450826.87359944	2728	124	0.6424	2.18	2.2
2450827.70428623	3653	163	0.0690	43.71	2.2
2450827.77446631	3653	342	0.1051	41.39	2.0
2450827.84209449	3644	151	0.1398	37.29	2.1

2450827.87402503	3674	122	0.1562	35.47	2.0
2450828.57683812	3643	158	0.5171	-6.92	2.0
2450828.59804605	3650	330	0.5280	-7.01	2.0
2450828.70171256	3643	310	0.5813	-4.48	1.7
2450828.82504772	3645	301	0.6446	1.91	2.3
2450828.86755618	3647	280	0.6664	4.78	1.9

MUSICOS, Nov 22, 1998 – Dec 13, 1998.

Site	HJD [24511+]	t_{exp} [s]	S/N	phase	v_r [km s ⁻¹]
OHP193	41.37584	1200	200	0.1549	35.1 ± 3.8
OHP193	41.48556	1200	190	0.2112	26.8 ± 3.1
OHP193	41.60501	1200	180	0.2726	23.4 ± 4.4
OHP193	44.37304	1800	170	0.6941	9.5 ± 3.1
OHP193	45.37442	1800	100	0.2083	27.3 ± 4.8
OHP193	46.36989	2100	210	0.7196	13.2 ± 3.6
OHP193	47.45078	2400	180	0.2747	16.2 ± 3.0
SAAO	(22:09)	1800	(80)	–	–
SAAO	(21:29)	924	–	–	–
SAAO	(21:13)	1800	(90)	–	–
SAAO	(00:52)	1800	–	–	–
BXO	49.25642	5400	30	0.2019	-6.4 ± 2.8
BXO	50.10649	3000	80	0.6385	61.8 ± 1.2
BXO	50.21550	3000	140	0.6945	69.9 ± 1.7
BXO	50.27836	3000	150	0.7268	75.3 ± 1.4
BXO	52.09376	3000	120	0.6591	3.2 ± 2.7
BXO	52.19891	3000	120	0.7131	12.3 ± 3.3
BXO	52.27990	3000	80	0.7547	18.3 ± 2.5
BXO	55.15105	2700	30	0.2291	49.7 ± 2.3
BXO	55.24648	3000	40	0.2781	48.6 ± 1.7
MSO	47.04042	1500	95	0.0639	49.3 ± 4.6
MSO	47.05919	1500	120	0.0736	49.7 ± 3.1
MSO	47.16410	1500	90	0.1274	43.3 ± 2.2
MSO	47.94040	1500	100	0.5261	0.6 ± 4.5
MSO	48.02403	1500	130	0.5691	0.9 ± 1.9
MSO	48.15425	1200	100	0.6359	6.9 ± 2.3
MSO	48.93913	1500	110	0.0390	51.3 ± 3.6
MSO	49.07460	1500	110	0.1086	45.7 ± 3.7
MSO	49.15082	1200	90	0.1477	39.8 ± 6.2
MSO	49.94285	1500	25	0.5545	-4.0 ± 6.4
MSO	50.98270	1500	105	0.0885	49.3 ± 3.3
MSO	51.04591	1200	110	0.1209	44.8 ± 2.6
MSO	51.10611	1200	110	0.1519	41.8 ± 3.6
KPNO	41.63019	1200	45	0.2855	–
KPNO	41.67969	1200	50	0.3109	–
KPNO	41.78911	1200	40	0.3671	–
KPNO	41.92587	1200	70	0.4373	–
KPNO	42.61928	1200	55	0.7934	–
KPNO	42.70574	1200	70	0.8378	–
KPNO	42.80249	1200	60	0.8875	–
KPNO	42.90963	1200	65	0.9426	–
KPNO	42.98487	1200	65	0.9812	–
KPNO	43.80302	1500	80	0.4014	–
KPNO	43.88231	1200	70	0.4421	–
KPNO	43.89726	1200	70	0.4498	–

5596.963	0.8251	27.63 KPNO/CF/TIF
5599.008	0.8753	36.25 KPNO/CF/TIF
5717.791	0.8762	34.75 KPNO/CF/TIF
5718.764	0.3759	1.83 KPNO/CF/TIF
5719.768	0.8915	39.83 KPNO/CF/TIF
5720.740	0.3907	-3.75 KPNO/CF/TIF
5721.727	0.8976	40.63 KPNO/CF/TIF
5941.958	0.9971	45.3 KPNO/CF/TIF
5971.996	0.4231	-7.11 KPNO/CF/TIF
6076.766	0.2276	21.99 KPNO/CF/TIF

Reference code:

D ... Donati et al. (1997)

F ... Fekel et al. (1987)

G ... Gunn et al. (1996)

S ... Strassmeier (1990)